Title
The effect of fluctuations on the helium-ionizing background

Journal
Monthly Notices of the Royal Astronomical Society, 437(2)

ISSN
0035-8711

Authors
Davies, Frederick B
Furlanetto, Steven R

Publication Date
2014-01-11

DOI
10.1093/mnras/stt1911

Peer reviewed

Mon. Not. R. Astron. Soc. **000**, 000–000 (0000) Printed 9 October 2013 (MN LATEX style file v2.2)

The Effect of Fluctuations on the Helium-Ionizing Background

Frederick B. Davies⋆, Steven R. Furlanetto†
Department of Physics & Astronomy, University of California, Los Angeles, Box 951547, Los Angeles, CA 90095

9 October 2013

ABSTRACT
Interpretation of He II Lyα absorption spectra after the epoch of He II reionization requires knowledge of the He II ionizing background. While past work has modelled the evolution of the average background, the standard cosmological radiative transfer technique assumes a uniform radiation field despite the discrete nature of the (rare) bright quasars that dominate the background. We implement a cosmological radiative transfer model that includes the most recent constraints on the ionizing spectra and luminosity function of quasars and the distribution of IGM absorbers. We also estimate, for the first time, the effects of fluctuations on the evolving continuum opacity in two ways: by incorporating the complete distribution of ionizing background amplitudes into the standard approach, and by explicitly treating the quasars as discrete – but isolated – sources. Our model results in a He II ionization rate that evolves steeply with redshift, increasing by a factor ~ 2 from $z = 3.0$ to $z = 2.5$. This causes rapid evolution in the mean He II Lyα optical depth – as recently observed – without appealing to the reionization of He II. The observed behaviour could instead result from rapid evolution in the mean free path of ionizing photons as the helium in higher H I column density absorbers becomes fully ionized.

Key words: cosmology: theory – intergalactic medium – diffuse radiation

1 INTRODUCTION

The ionizing background is crucial for understanding many aspects of large-scale structure and galaxy formation at high redshifts. For example, unraveling the physical density structure of the Lyα forest (which contains most of the the intergalactic medium, or IGM, at $z \gtrsim 2$) requires knowledge of the ionization state of the intervening material (Rauch 1998; Meiksin 2009). It is also crucial for understanding the abundance and distribution of heavy elements in the IGM, whose ionization states depend sensitively on the local metagalactic radiation field (e.g., Songaila 1998, 2005; Kim et al. 2002b; Aguirre et al. 2004; Bolton & Viel 2011). Additionally, the ionizing background is an important input parameter for cosmological simulations because it regulates the dominant heating and cooling in the IGM (Davé et al. 1999; Springel & Hernquist 2003), which forms the fuel supply for later galaxy formation. Finally, the ionizing background holds important clues about galaxies and quasars, because they are the dominant sources behind it. Precise measurements can constrain the star formation rate, the escape fraction of ionizing photons from galaxies, and the importance of luminous quasars (Madau et al. 1999; Faucher-Giguère et al. 2008a, 2009; Haardt & Madau 2012).

Perhaps most importantly, the ionizing background is tied inextricably to the reionization process, when the global ionization state of intergalactic atoms changes rapidly. For example, measurements of the H I ionizing background at $z \sim 5$–6 show that hydrogen reionization appears to proceed relatively slowly (Bolton & Haehnelt 2007). Its properties will also be crucial for understanding He II reionization, which is due to bright quasars (Sokasian et al. 2003; Furlanetto & Oh 2008; McQuinn et al. 2009). Based on studies of the effective optical depth of the He II Lyα forest, the reionization of He II in the universe seems to have completed at $z \sim 3$ (Reimers et al. 1997; Kriss et al. 2001; Zheng et al. 2004; Shull et al. 2004). The evolution of the ionizing background during and after He II reionization is critical to interpreting new and upcoming He II Lyα forest results from *HST/COS* (Shull et al. 2010; Worseck et al. 2011; Syphers et al. 2012). Theoretical calculations have attempted to address this evolution by semi-analytic modelling (Dixon & Furlanetto 2009; Furlanetto & Dixon 2010) and hydrodynamic simulations of the IGM (Sokasian et al. 2003; Bolton et al. 2006; Paschos et al. 2007; McQuinn et al. 2009).

There is a long history of calculations to estimate the properties of the metagalactic ionizing radiation field. Haardt & Madau (1996) made a landmark study of the ionizing background using a cosmological radiative transfer model for ionizing photons traveling through a clumpy IGM. By combining state-of-the-art constraints on the distribution of ionizing sources and the absorber distribution of the IGM, Haardt & Madau (1996) were able to compute the evolving ionizing background of H I and He II. Further studies (Fardal et al. 1998; Faucher-Giguère et al. 2009; Haardt & Madau 2012) have updated this framework with new constraints on the population of ionizing sources and the distribution and properties

⋆ davies@astro.ucla.edu
† sfurlane@astro.ucla.edu

of IGM absorbers. However, all of these studies treated the ionizing background (and its sources and sinks) as *uniform* components, which is a reasonable approximation for the H I background (at least at low and moderate redshifts; Meiksin & White 2004) but is a poor approximation when bright, rare sources dominate the emissivity (as is the case for quasars and the He II ionizing background).

Fardal et al. (1998) showed how the relatively large mean separation of He II ionizing sources could contribute to the significant observed fluctuations in the ionizing background and hence in the observable He II Lyα effective optical depth. An analytic description of variations in the metagalactic radiation field was introduced by Zuo (1992), expanded by Meiksin & White (2003), and later used by Furlanetto (2009) to study fluctuations in the He II ionizing background. Despite this theoretical interest, there has been no effort to include the effect of these fluctuations on the ionizing continuum opacity within a cosmological radiative transfer model. In this work, we attempt to show the self-consistent effect of these fluctuations on the mean ionizing background.

We begin in Section 2 with a description of our implementation of a cosmological radiative transfer model to calculate self-consistently the He II ionization rate. Then, in Section 3, we present the results of our model. In Section 4, we use the results from that model to calculate the evolution of the He II effective optical depth and compare it to observations. We discuss our model assumptions and compare to previous work in Section 5. We conclude in Section 6.

In our calculations, we assume the following cosmology: $\Omega_m = 0.26$, $\Omega_\Lambda = 0.74$, $\Omega_b = 0.044$, and $h = 0.74$ (Dunkley et al. 2009). All distances are given in comoving units unless otherwise specified.

2 INPUTS/METHODS

2.1 Cosmological Radiative Transfer

To calculate the He II ionizing background, we employ a cosmological radiative transfer model (Haardt & Madau 1996). By considering photon conservation in a comoving volume element, the specific intensity of ionizing radiation J_ν behaves as

$$\left(\frac{\partial}{\partial t} - \nu H \frac{\partial}{\partial \nu}\right) J_\nu = -3HJ_\nu - c\alpha_\nu J_\nu + \frac{c}{4\pi}\epsilon_\nu, \quad (1)$$

where $H(t)$ is the Hubble parameter, c is the speed of light, α_ν is the absorption coefficient (with $d\tau_\nu = \alpha_\nu dl$ and dl the proper line element), and ϵ_ν is the proper emissivity. This approach assumes that each volume element can be described as an isotropic source and sink of radiation through ϵ_ν and α_ν, respectively: we will revisit this assumption later on. The solution to the cosmological radiative transfer equation is

$$J_{\nu_0}(z_0) = \frac{1}{4\pi}\int_{z_0}^{\infty} dz \frac{dl}{dz}\frac{(1+z_0)^3}{(1+z)^3}\epsilon_\nu(z)\exp[-\bar{\tau}(\nu_0, z_0, z)]. \quad (2)$$

where $dl/dz = c/((1+z)H(z))$ is the proper line element, $\nu = \nu_0(1+z)/(1+z_0)$, and $\bar{\tau}$ is the effective optical depth experienced by a photon at frequency ν_0 and redshift z_0 since its emission at redshift z. $\bar{\tau}$ is calculated using $e^{-\bar{\tau}} = \langle e^{-\tau}\rangle$ averaging over all lines of sight. For Poisson-distributed absorbers with H I column density $N_{\rm H\,I}$ this opacity is (Paresce et al. 1980)

$$\bar{\tau}(\nu_0, z_0, z) = \int_{z_0}^{z} dz' \int_0^\infty dN_{\rm H\,I} \frac{\partial^2 N}{\partial N_{\rm H\,I}\partial z'}(1 - e^{-\tau_\nu}), \quad (3)$$

where $\partial^2 N/\partial N_{\rm H\,I}\partial z \equiv f(N_{\rm H\,I}, z)$ is the column density distribution function (CDDF) of neutral hydrogen absorbers. The most common simple form of the CDDF is a power law in column density and redshift: $f(N_{\rm H\,I}, z) \propto N_{\rm H\,I}^{-\beta}(1+z)^\gamma$, but we will allow more sophisticated models as well (see § 2.5.3).

The optical depth of an absorber to ionizing photons of frequency ν is given by

$$\tau_\nu = N_{\rm H\,I}\sigma_{\rm H\,I}(\nu) + N_{\rm He\,I}\sigma_{\rm He\,I}(\nu) + N_{\rm He\,II}\sigma_{\rm He\,II}(\nu), \quad (4)$$

where N_i are the column densities and σ_i are the photoionization cross-sections of ion i. Because only the column density distribution of $N_{\rm H\,I}$ has been measured, we use a model for the relationship between $N_{\rm H\,I}$ and $N_{\rm He\,II}$ to calculate the He II ionizing opacity (see § 2.1.1). In the frequency range contributing to the He II ionizing background ($\nu > \nu_{\rm He\,II} = 4\,\nu_{\rm H\,I}$) we assume the contribution to the optical depth from He I is negligible following Faucher-Giguère et al. (2009). Finally, the ionization rate for He II is given by

$$\Gamma_{\rm He\,II}(z) = 4\pi\int_{\nu_{\rm He\,II}}^{\infty}\frac{J_\nu(z)}{h\nu}\sigma_{\rm He\,II}(\nu)d\nu, \quad (5)$$

where $\nu_{\rm He\,II}$ is the ionization threshold of He II.

In our model, we do not explicitly calculate the H I ionization rate, as that calculation depends strongly on poorly constrained models of the escape fraction of ionizing photons from star-forming galaxies (see e.g. Haardt & Madau 2012). Because the detailed evolution of $\Gamma_{\rm H\,I}$ is not the focus of this work, we instead adopt an empirical estimate of the H I ionization rate from measurements of the Lyα forest (Faucher-Giguère et al. 2008a), which appears to be fairly constant over our redshift range of interest ($z \sim$ 2–4). We have ensured that our fiducial value for $\Gamma_{\rm H\,I}$ is consistent with our fiducial quasar emissivity and CDDF; that is, the value of $\Gamma_{\rm H\,I}$ calculated in our fiducial model with quasars only is less than the value we assume in the fiducial $\Gamma_{\rm He\,II}$ calculation.

Because the ionizing background and the continuum opacity are interrelated through the conversion of $N_{\rm H\,I}$ to $N_{\rm He\,II}$ described in the next section, the procedure must be iterated over the entire redshift range until convergence. The result of this cosmological radiative transfer model as presented in this section will be referred to as the "uniform" background model in the rest of the paper.

2.1.1 *Absorber Ionization Structure: $N_{\rm H\,I}$ to $N_{\rm He\,II}$*

The relationship between $N_{\rm H\,I}$ and $N_{\rm He\,II}$ is usually parameterized by the quantity $\eta = N_{\rm He\,II}/N_{\rm H\,I}$ (Miralda-Escude 1993). In the optically thin case, η is given by

$$\eta_{\rm thin} = \frac{\Gamma_{\rm H\,I}}{\Gamma_{\rm He\,II}}\frac{\alpha^A_{\rm He\,II}}{\alpha^A_{\rm H\,I}}\frac{Y}{4X}, \quad (6)$$

where $\alpha^A_{\rm H\,I}$ and $\alpha^A_{\rm He\,II}$ are the case-A recombination coefficients of H I and He II , and $X = 0.75$ and $Y = 0.25$ are the hydrogen and helium mass fractions, respectively. In an optically thin environment, photons produced by recombinations to the ground state of He II will escape from the local medium, hence our choice of case-A recombination coefficients. Note, however, that these coefficients enter only in the ratio, so this choice does not have any significant effect.

To more generally translate H I column densities into He II , we adopt a fit to numerical simulations that accounts for self-shielding in neutral hydrogen systems (Fardal et al. 1998; Faucher-Giguère et al. 2009),

$$\frac{Y}{16X}\frac{\tau_{\rm H\,I}}{1+A\tau_{\rm H\,I}}I_{\rm H\,I}=\tau_{\rm He\,II}+\frac{\tau_{\rm He\,II}}{1+B\tau_{\rm He\,II}}I_{\rm He\,II}, \quad (7)$$

where $\tau_i=\sigma_i N_i$, $A=0.15$ and $B=0.2$ are fitting coefficients used by Faucher-Giguère et al. (2009), and $I_i=\Gamma_i/n_e\alpha_i^A$ with $n_e=1.4\times10^{-3}$ cm$^{-3}(N_{\rm H\,I}/10^{17.2}$ cm$^{-2})^{2/3}(\Gamma_{\rm H\,I}/10^{-12}$ s$^{-1})^{2/3}$ (Schaye 2001). At small H I column densities ($N_{\rm H\,I}\lesssim10^{15}$ cm^{-2}), $N_{\rm He\,II}=\eta_{\rm thin}N_{\rm H\,I}$ as expected. He II becomes optically thick to ionizing radiation for larger column densities ($N_{\rm H\,I}\sim10^{15}$–10^{17} cm^{-2}), so η increases by a factor of a few as more He II forms while hydrogen remains highly ionized. Then, for $N_{\rm H\,I}\gtrsim10^{17}$ cm^{-2}, η steeply drops as the systems become optically thick to H I ionizing photons.

For systems with $N_{\rm H\,I}>10^{18}$ cm^{-2}, the numerical fit systematically under-predicts the amount of He II from the original model (see Figure 1 of Faucher-Giguère et al. 2009). For frequencies near $\nu_{\rm He\,II}$, the opacity is unaffected because these high $N_{\rm H\,I}$ systems are still optically thick due to H I absorption. However, for $\nu\gtrsim2.5\,\nu_{\rm He\,II}$, absorbers with $N_{\rm H\,I}\sim10^{19}$–10^{20} cm^{-2} start to become optically thin due to their relative lack of He II . Fortunately, the total ionization rate only changes slightly because the range of affected column densities is small and the vast majority of ionizations occur at lower frequencies ($\sigma_{\rm He\,II}\propto\nu^{-3}$).

Haardt & Madau (2012) applied a similar method to fit the absorber structure that considers the average Γ within absorbers instead of the external "optically-thin" Γ. While their method provides a better fit to the numerical models at $N_{\rm H\,I}>10^{18}$ cm^{-2}, it differs from the Faucher-Giguère et al. (2009) model only in the details for the more important $\tau_{\rm He\,II}\sim1$ ($N_{\rm H\,I}\sim10^{16}$ cm^{-2}) absorbers. This is an example of one of the systematic uncertainties in our procedure: these models for η must assume physical characteristics for the absorbers (densities, temperatures, and geometry, for example) that are both uncertain and simplifications of the true IGM physics. For concreteness, the numerical absorber model from Faucher-Giguère et al. (2009) assumes uniform density semi-infinite slabs with a thickness determined by the local Jeans length (at $T=20,000$ K) in photoionization equilibrium with both an external radiation background and internal recombination processes.

2.1.2 Recombination Emissivity

Recombinations of He III to the ground state of He II will produce ionizing continuum radiation. Although the recombination rate in a uniform density medium can easily be estimated from ionization equilibrium, the real universe requires a more detailed approach for two reasons. First, density inhomogeneities in the IGM substantially boost the recombination rate. We can model this by integrating over the H I column density distribution of the Lyα forest. Second, recombination photons produced inside optically thick absorbers will not escape to affect the IGM.

We model the recombination emissivity of IGM absorbers with a numerical fit to the radiative transfer models of Faucher-Giguère et al. (2009). The emergent specific intensity from an absorber with He II column density $N_{\rm He\,II}$ can be approximated by

$$I_\nu^{\rm rec}(N_{\rm He\,II})=\frac{h\nu}{4\pi}\left(1-\frac{\alpha^B_{\rm He\,II}}{\alpha^A_{\rm He\,II}}\right)\Gamma_{\rm He\,II}\phi_{\nu,\rm rec}\times N_T\left(1-e^{N_{\rm He\,II}/N_T}\right), \quad (8)$$

where the second factor is the fraction of ionizations to the ground state and the local ionization rate is $\Gamma_{\rm He\,II}$. $N_T=10^{17.3}$ cm^{-2} is the approximate threshold He II column density above which the emission becomes saturated by absorption within the absorber itself (the decline at larger columns is approximated by the last factor). $\phi_{\nu,\rm rec}$ is the normalized recombination emission profile:

$$\phi_{\nu,\rm rec}\propto\nu^{-1}e^{-h\nu/k_BT}\theta(\nu-\nu_{\rm He\,II}), \quad (9)$$

where $\theta(x)$ is the Heaviside step function. The effective frequency width of this emission is $\Delta\nu/\nu\sim k_BT/h\nu_{\rm He\,II}\sim0.03$, which limits the distance these photons can travel to $\lesssim30$ Mpc before redshifting below the He II ionizing edge.

The total proper emissivity from recombinations is then

$$\epsilon_{\nu,\rm rec}(z)=\frac{dz}{dl}\int_0^\infty dN_{\rm H\,I}\,f(N_{\rm H\,I},z)\,4\pi I_\nu^{\rm rec}(N_{\rm He\,II}), \quad (10)$$

where the intensity depends implicitly on $N_{\rm H\,I}$ through the conversion factor η. We include the recombination emissivity in the cosmological radiative transfer calculation by simply adding it to the emissivity from quasars, ignoring the difference in spatial distribution.

We note here that the recombination photons can have a much larger effect on the ionizing background than one might naively expect from their emissivity. As we shall see later, increasing the emissivity also increases the mean free path of ionizing photons, which amplifies the effect of the additional ionizing photons. We will explore this issue further in § 3.1.5.

2.2 Mean Free Path

The opacity per unit redshift, $d\bar\tau/dz$, was integrated in equation (3) to calculate the total opacity between two redshifts:

$$\frac{d\bar\tau}{dz}=\int_0^\infty dN_{\rm H\,I}f(N_{\rm H\,I},z)(1-e^{-\tau_\nu(\Gamma_{\rm He\,II})}), \quad (11)$$

where the absorber opacity as a function of $N_{\rm H\,I}$, τ_ν, depends on $\Gamma_{\rm He\,II}$ through the absorber model in Section 2.1.1. At a given redshift, $d\bar\tau/dz$ describes the local opacity due to the forest of individual absorbers in the IGM. By inverting this quantity and converting from redshift difference to a comoving distance, we find the distance per unit optical depth, which is simply the mean free path:

$$\lambda_{\rm mfp}(\nu,z)=\frac{dl}{dz}\left(\frac{d\bar\tau}{dz}\right)^{-1}. \quad (12)$$

If $f(N_i,z)=N_0N_i^{-\beta}(1+z)^\gamma$ and $\sigma_i=\sigma_0(\nu/\nu_i)^{-3}$, the comoving mean free path reduces to

$$\lambda_{\rm mfp}(\nu,z)\approx\frac{(\beta-1)c}{\Gamma_G(2-\beta)N_0\sigma_0^{\beta-1}}\left(\frac{\nu}{\nu_i}\right)^{3(\beta-1)}\times\frac{1}{(1+z)^\gamma H(z)}, \quad (13)$$

where Γ_G is the Gamma function. The redshift dependence of the mean free path in this simplified model is then $\lambda_{\rm mfp}\propto(1+z)^{-(\gamma+1.5)}$. This power law dependence is a good approximation to describe the evolution of the mean free path of H I ionizing photons ($\lambda_{\rm H\,I}$) in our model because the H I CDDF is fixed, but we find that it fails to capture the more complicated $\Gamma_{\rm He\,II}$-dependent evolution of the mean free path of He II ionizing photons ($\lambda_{\rm He\,II}$; see § 3.1.4).

Recent efforts by Prochaska et al. (2009) and O'Meara et al. (2013) have directly measured the H I ionizing mean free path of the IGM near $z\sim4$ and $z\sim2$ respectively. For an identical distribution of absorbers, they would report different values than obtained by our approach because they define the mean free path as

the distance traveled by a photon through the *evolving* IGM while it redshifts with the cosmic expansion, rather than the path that could be traveled if the IGM and photon retained their original properties (as is the usual definition for theoretical work). We follow the latter definition here.

2.3 Fluctuations

In a smooth, fully-ionized IGM, the intensity of ionizing radiation from an individual quasar falls as $\exp[-r/\lambda_{\rm mfp}]/r^2$. Given a distribution of quasar luminosities and a mean free path, a probability distribution of intensities can be computed assuming random placement of quasars following Poisson statistics (Zuo 1992; Meiksin & White 2003). The effects of this distribution on the *mean* ionizing background have not previously been considered. The next stage in our model is therefore to incorporate the distribution (in a somewhat ad hoc manner) in order to understand better the implications of this fluctuating background.

We use the Hopkins et al. (2007) B-band quasar luminosity function (QLF) to describe the distribution of relative quasar luminosities, assuming an average quasar spectral energy distribution such that the specific luminosity at the H I ionizing edge is proportional to the B-band specific luminosity (L_B), then extrapolating to the He II ionizing edge by a spectral index α. Additionally, while the effect is relatively minor (Furlanetto 2009), we convolve the quasar luminosity function with a distribution of far-ultraviolet spectral indices that roughly matches observations by Telfer et al. (2002): a Gaussian distribution over $0.5 < \alpha < 3.5$ with central value $\bar{\alpha} = 1.5$ and $\sigma_\alpha = 0.7$. Note that the asymmetric bounds on α lead to an average spectral index of $\alpha \simeq 1.6$ consistent with our fiducial value (described later in § 2.5.1). In detail, the average ratio between the emissivity at 1 and 4 Ryd will be somewhat higher than the ratio for a $\alpha = 1.6$ spectrum, but we fold this uncertainty into the ionizing background normalization uncertainty described in § 3.

We use the method of characteristic functions from Meiksin & White (2003) to determine the probability distribution of intensity, $f(J)$, then scale linearly to Γ by $\Gamma = J \times \langle\Gamma\rangle/\langle J\rangle$ (Furlanetto 2009). The last assumption of proportionality between the intensity of radiation and the ionization rate is not strictly true; the intensity at higher frequencies should be more uniform because the mean free path is much larger, although the effect is modest in practice (Dixon et al. 2013). In our calculation of $f(\Gamma)$ we use the mean free path of the "average" He II ionizing photon, $\bar{\lambda}_{\rm HeII} = \lambda_{\rm mfp}(\bar{\nu})$, where $\bar{\nu}$ is defined by

$$\bar{\nu}\Gamma_{\rm He\,II} = 4\pi \int_{\nu_{\rm He\,II}}^{\infty} \nu \times \frac{J_\nu(z)}{h\nu}\sigma_{\rm He\,II}(\nu)d\nu, \quad (14)$$

in an attempt to average over the frequency dependence of the background fluctuations. In general, $\bar{\lambda}_{\rm He\,II}$ is substantially larger than $\lambda_{\rm He\,II}$, so our approach provides a conservative estimate when used to calculate the amplitude of ionizing background fluctuations.

Figure 1 shows how the $f(\Gamma)$ distribution varies with mean free path. When the mean free path decreases, the peak of the distribution skews towards smaller Γ relative to the mean. For Γ below the mean, we find that the He II opacity of each absorber will increase, with the total opacity increasing as, roughly, $d\bar{\tau}/dz \propto \Gamma^{-2/3}$ using the He II absorber model of Section 2.1.1. Because this relationship between the ionization rate and opacity is more gentle than linear, the skewness of the $f(\Gamma)$ distribution results in an average opacity that is *higher* than the opacity at the mean Γ.

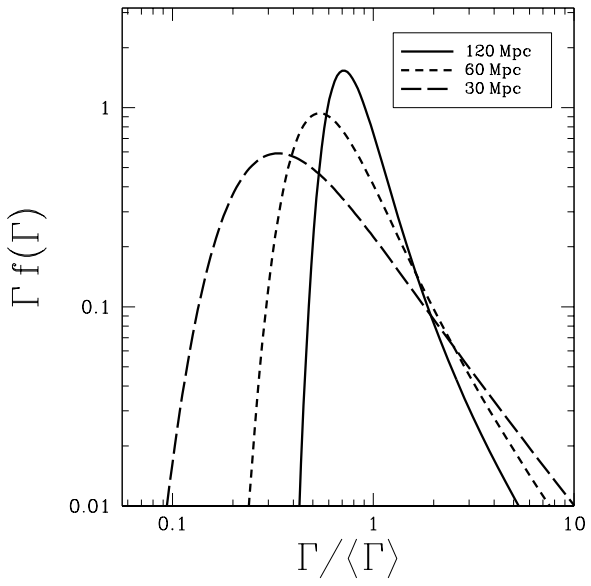

Figure 1. Distribution of ionization rates at $z = 3.0$ for $\lambda_{\rm mfp} = 30, 60, 120$ Mpc (long-dashed, dashed, and solid, respectively).

That is, the lower opacity in rare high Γ regions does not counteract the higher opacity in common low Γ regions. We explore this effect in the following discussion.

We incorporate these fluctuations into our ionizing background model by averaging the opacity $d\bar{\tau}/dz$ (equations 3, 11) over the distribution $f(\Gamma)$:

$$\left\langle \frac{d\bar{\tau}}{dz} \right\rangle = \int_0^\infty \frac{d\bar{\tau}}{dz}(\Gamma) f(\Gamma) d\Gamma, \quad (15)$$

where $d\bar{\tau}/dz$ depends on Γ through the absorber prescription in Section 2.1.1 and $f(\Gamma)$ is initialized with the mean free path calculated in the uniform model. This process is repeated using the same $f(\Gamma)$ for each frequency in equations (2) and (5) to modify the ionizing continuum opacity at each redshift. The fractional increase in the opacity due to the integral over $f(\Gamma)$ is larger for smaller $\lambda_{\rm mfp}$, reaching $\sim 40\%$ in our fiducial model if $\lambda_{\rm mfp}$ is equal to the average distance between bright sources at $z = 3$ (~ 45 Mpc; see §3.2). Because the modified opacity leads to new values for $\Gamma_{\rm He\,II}(z)$ and $\lambda_{\rm mfp}(z)$, we iterate this process using the new $\lambda_{\rm mfp}(z)$ to generate $f(\Gamma)$ and using the new $\Gamma_{\rm He\,II}(z)$ to calculate $d\bar{\tau}/dz(\Gamma, z)$.

Unfortunately, as presented above, the $\Gamma_{\rm He\,II}$ calculation does not converge to a non-zero value; the added opacity from the $f(\Gamma)$ prescription causes the iterative procedure to drive $\Gamma_{\rm He\,II}$ down to zero. At relatively high redshifts ($z \gtrsim 3.5$) the mean free path is short enough ($\lambda_{\rm mfp} \lesssim 50$ Mpc) that integrating over $f(\Gamma)$ greatly increases the opacity. In practice, this increased opacity at high redshift propagates small values of $\Gamma_{\rm He\,II}$ to lower redshifts, and the iterative effect pulls Γ down to zero at *all* redshifts. Even when the ionizing background is calculated assuming local emission and absorption of photons (i.e. without an integral over redshift as in equation 2) via the absorption-limited approximation $J_\nu(z) = \epsilon_\nu(z)\lambda_{\rm mfp}(\nu, z)/(4\pi)$ (Meiksin & White 2003), the divergence to zero remains at $z \gtrsim 3.2$.

The reason our procedure breaks down is actually obvious: our cosmological radiative transfer model assumes that ionizing photons are emitted uniformly throughout the universe (with a con-

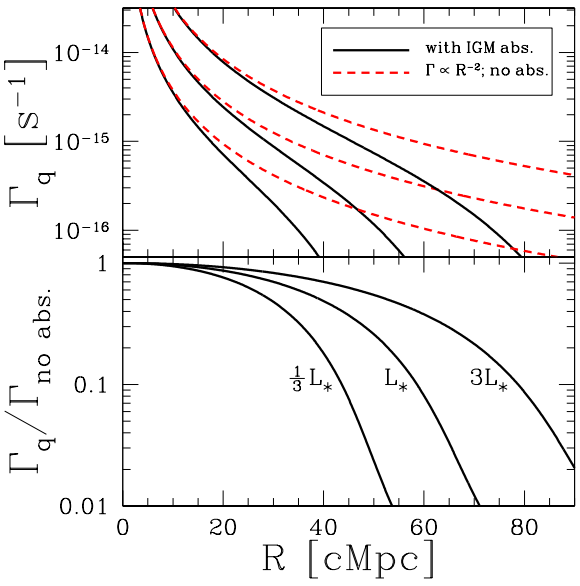

Figure 2. Line-of-sight equilibrium ionization rate profile for $L = 1/3\ L_*, L_*, 3L_*$ (from bottom to top) quasars at $z = 3$ with IGM continuum absorption (solid black) and without (dashed red). In all cases, the quasars are assumed to be isolated (i.e., with no contribution from a metagalactic background).

stant ϵ_ν in equation 1), but the real quasar sources are of course point-like. Since the ionizing background near a source is much stronger than the average, the local IGM will be less opaque to ionizing photons, and the quasar photons will penetrate farther into the IGM – increasing the ionizing background. Additionally, our model assumes that the path traversed by an ionizing photon fully samples the distribution of ionization rates given by $f(\Gamma)$, but within a quasar proximity region this is not accurate, as the radiation profile is smoothly decreasing. To quantify the minimum effect these transparent proximity regions must have on the mean background, we consider a simple model where the ionizing background is calculated as the sum of isolated source ionization rate profiles.[1]

2.4 Minimum Background Model

In the absence of an external ionizing background and ignoring the cosmological redshift of ionizing photons, the equilibrium ionization rate profile along a sightline from a single quasar, $\Gamma_q(R)$, is given by

$$\Gamma_q(R) = \int_{\nu_{\rm He\,II}}^{\infty} \frac{L_\nu}{4\pi R^2 h\nu}\sigma_\nu \exp[-\tau_\nu(R)]d\nu, \qquad (16)$$

where $\tau_\nu(R)$ is the optical depth at frequency ν from the IGM at $r < R$,

$$\tau_\nu(R) = \int_0^R \frac{d\tau}{dz}(\nu, \Gamma_q(r))(\frac{dl}{dz})^{-1}dr, \qquad (17)$$

and assuming $L_\nu \propto \nu^{-1.6}$ as the mean quasar spectrum for simplicity.

Figure 2 shows the ionization rate profiles for $L = 1/3\ L_*, L_*, 3L_*$ quasars (from bottom to top) at $z = 3$. At small radii, the effective mean free path is very large, so $\Gamma_q \sim R^{-2}$. However, once Γ_q is small enough such that $R \sim \lambda_{\rm mfp}(\Gamma_q)$, the ionization rate drops sharply. Thus, each quasar has a characteristic radius beyond which it generates very few ionizations, effectively a recombination-limited "proximity zone."

This ionization rate profile, integrated from small to large radius, can be calculated without detailed radiative transfer because all of the ionization state and absorption properties are contained in our prescription for the clumpy IGM through the CDDF and absorber structure from Section 2.1.1. In a physical sightline, the attenuation in the IGM will be dominated by random encounters with absorbing clouds, so a more accurate description could be obtained by radiative transfer through a realistic IGM density field. We assume ionization equilibrium in the average IGM for simplicity.

The sum of these isolated quasar profiles should provide a *minimal* estimate of the mean background consistent with the CDDF and the QLF, because they ignore collective effects from the overlap of the proximity zones. Armed with the Γ_q profiles as a function of quasar luminosity, we can calculate this minimum mean background by integrating over the QLF and averaging over position,

$$\Gamma_{\rm min} = \int_0^\infty \left(\int_{L_{\rm min}}^\infty \Gamma_q(R, L)\Phi(L)dL\right) 4\pi R^2 dR, \qquad (18)$$

where $\Phi(L)$ is the Hopkins et al. (2007) QLF and $L_{\rm min}$ is the smallest luminosity quasar that we consider ($L_{\rm min} = 10^{43}$erg s^{-1} in the B-band, but the overall results do not depend strongly on this choice). The majority of $\Gamma_{\rm min}$ comes from cosmologically local sources (within $\sim$ 75 cMpc), so neglecting the cosmological redshift of ionizing photons should be a reasonable approximation. The resulting $\Gamma_{\rm min}(z)$ will be referred to as the "minimum" background model in the rest of the paper. We will see in Section 3 that the minimum model ionization rate is nearly constant over the redshift range we consider.

In our model, the minimum background provides a maximum average opacity for the IGM. To implement the minimum background into our modified cosmological radiative transfer model, we make the following approximation: when determining the opacity $d\tau/dz$ at a given redshift, use the larger of $\Gamma_{\rm He\,II}(z)$ and $\Gamma_{\rm min}(z)$.[2] The minimum background model is not meant to represent a universe where there is a floor in the ionizing background at any point in space, but rather one where the *average* ionizing background has a floor based on the proximity effects of rare bright sources. This model could be similar to the pre-reionization universe, where the average ionizing background is dominated by expanding ionized bubbles around such sources. While the difference between this highly fluctuating (by construction) background and the pre-reionization universe is subtle, in practice we find that distinction does not matter for our purposes. In the regime where the minimum background model dominates our results, the behaviour of the ionizing background is unlikely to be well-described by glob-

[1] For simplicity, we will ignore the finite lifetimes of quasars in our calculation. In reality, these finite lifetimes limit the extent of an individual quasar's radiation field. However, the radiation field will continue to propagate outward even after the quasar shuts off, following the profile that we describe here. The statistical results we describe here are therefore unaffected by a finite lifetime.

[2] This discontinuity in the opacity calculation results in a slight redshift discontinuity in the ionizing background evolution, but as mentioned in the text, the mean background we calculate in this regime is unlikely to be physically relevant.

ally averaged quantities, so we focus our analysis at redshifts when $\Gamma > \Gamma_{\rm min}$.

The results of this modified cosmological radiative transfer model will be referred to as the "fluctuating" background model in the rest of the paper.

2.4.1 *Summary of Fluctuating Method*

In summary, we calculate the fluctuating background model in the following manner:

(i) Initialize $\Gamma_{\rm He\,II}(z)$ and $\lambda_{\rm mfp}(z)$ using the standard cosmological radiative transfer approach (equations 2–5, 11–12).
(ii) Calculate $f(\Gamma)$ as a function of redshift using $\lambda_{\rm mfp}(z)$ as input to the method of Furlanetto (2009).
(iii) Calculate the average opacity $\langle d\bar{\tau}/dz\rangle$ as a function of redshift using $f(\Gamma)$ (equation 15).
(iv) Calculate $\Gamma_{\rm He\,II}(z)$ with equations 2–5 using $\langle d\bar{\tau}/dz\rangle$ in equation 3.
(v) Calculate $\lambda_{\rm mfp}(z)$ with equations 11–12, substituting $\langle d\bar{\tau}/dz\rangle$ for $d\bar{\tau}/dz$ in equation 12.
(vi) Repeat steps (ii)–(v) until $\Gamma_{\rm He\,II}(z)$ converges.

2.5 Model Input Parameters

Other than our simple model assumptions, the largest sources of uncertainty in our analysis are three observed parameters: the He II ionizing emissivity, ϵ_ν, the H I ionization rate, $\Gamma_{\rm H\,I}$, and the neutral hydrogen column density distribution, $f(N_{\rm H\,I}, z)$. In this section, we discuss the range of observed values for these parameters.

2.5.1 *He II Ionizing Emissivity*

We adopt the Lyman limit quasar ionizing emissivity from Haardt & Madau (2012),

$$\epsilon_{912}(z) = 10^{24.6}{\rm erg\,s^{-1}\,Mpc^{-3}\,Hz^{-1}} \times(1+z)^{4.68}\frac{\exp[-0.28z]}{\exp[1.77z]+26.3}, \quad (19)$$

which is a fit to the integrated B-band quasar luminosity function of Hopkins et al. (2007) converted to $\nu_{\rm H\,I}$ by a constant factor,

$$L_{\nu_{\rm H\,I}} = L_B \times 10^{18.15}{\rm erg\,s^{-1}\,Hz^{-1}}\left(\frac{L_\odot}{L_B}\right). \quad (20)$$

This factor is effectively an estimate of the average quasar spectrum between ν_B and $\nu_{\rm H\,I}$. For frequencies above the Lyman limit, we assume a power law spectrum with $\epsilon_\nu \propto \nu^{-\alpha}$. For reference, the integrated quasar emissivity given by equation (19) increases by $\sim 30\%$ from $z = 3$–2.

The uncertainty in the He II ionizing emissivity is a combination of the uncertainty in the Hopkins et al. (2007) quasar luminosity function and the assumed average quasar spectrum. The former is likely to be small, because the integrated quasar B-band emissivity at $z \gtrsim 2$ comes predominantly from the brightest, and therefore best measured, sources (Hopkins et al. 2007). The latter uncertainty is dominated by the choice of far-UV spectral index α. Telfer et al. (2002) find $\alpha = 1.57 \pm 0.17$ for a composite spectrum of 77 radio-quiet quasars, while the composite including an additional 107 radio-loud quasars has $\alpha = 1.76\pm0.12$. In contrast, Scott et al. (2004) found that the average spectral index for their sample of 85 sources was considerably harder, $\alpha = 0.56^{+0.28}_{-0.38}$. Shull et al. (2012) measured a best-fit spectral index of $\alpha = 1.41 \pm 0.21$ for their sample of 22 sources using *HST/COS*.

We adopt $\alpha = 1.6$ as our fiducial value. Note that, because the He II Lyman limit $\nu_{\rm He\,II} = 4\nu_{\rm H\,I}$, a change in the spectral index $\Delta\alpha$ corresponds to a factor of $4^{-\Delta\alpha}$ difference in the emissivity at $\nu_{\rm He\,II}$.

2.5.2 *H I Ionization Rate*

The absorber model in § 2.1.1 depends on the H I ionization rate, $\Gamma_{\rm H\,I}$. Measurements of $\Gamma_{\rm H\,I}$ from $z \sim$ 2–3 yield values $\sim 0.5 - 1.0 \times 10^{-12}$ s^{-1} from flux decrement observations (Rauch et al. 1997; Bolton et al. 2005; McDonald & Miralda-Escudé 2001; Faucher-Giguère et al. 2008a) or $\sim 1.0 - 3.0 \times 10^{-12}$ s^{-1} from proximity effect measurements (Scott et al. 2000). The most recent cosmological radiative transfer model by Haardt & Madau (2012) suggests $\Gamma_{\rm H\,I} \sim 0.8 - 0.9 \times 10^{-12}$ s^{-1}, but as discussed in the next section, that study may have significantly underestimated the total H I opacity of the IGM. We adopt $\Gamma_{\rm H\,I} = 0.6 \times 10^{-12}$ s^{-1}, a value consistent with the measurements of Faucher-Giguère et al. (2008a), as our fiducial value but consider a range of plausible values.

2.5.3 *Column Density Distribution*

The column density distribution of neutral hydrogen $f(N_{\rm H\,I}, z) = \partial^2 N/\partial N_{\rm H\,I}\partial z$ has been measured several times and over a range of redshifts through observations of the H I Lyα forest. Early observations indicated that the $N_{\rm H\,I}$ distribution is well-fit by a power law of the form $f(N_{\rm H\,I}) \propto N_{\rm H\,I}^{-\beta}$ with $\beta \sim 1.5$ over a wide range of observed column densities ($10^{12} < N_{\rm H\,I} < 10^{22}$ cm^{-2}) and redshifts ($z \sim$ 0.2–3.5) (Tytler 1987). Recent studies of H I ionizing continuum opacity in stacked quasar spectra at $z \sim 2$ and $z \sim 4$ suggest a deficit of Lyman limit systems ($10^{17.2} < N_{\rm H\,I} < 10^{19}$ cm^{-2}; LLS) and intermediate H I column density systems ($10^{15} < N_{\rm H\,I} < 10^{17.2}$ cm^{-2}) relative to the canonical single power law model, and several authors have proposed multi-step power law distributions to describe this feature (Prochaska et al. 2009, 2010; Worseck & Prochaska 2011; O'Meara et al. 2013; Haardt & Madau 2012). Rudie et al. (2013) performed the largest survey of $10^{12} < N_{\rm H\,I} < 10^{17.2}$ cm^{-2} systems to date for redshifts $z = 2.02$–2.84 ($\langle z\rangle \sim 2.4$) and found no evidence of the deficit suggested by stacked quasar spectra studies. They found that their measured distribution is well-parameterized by a relatively steep $\beta \sim 1.66$ power law for $N_{\rm H\,I} \lesssim 10^{15}$ cm^{-2} and a $\beta \sim 1.48$ power law for larger H I column densities. The left panel of Figure 3 shows several of these distributions graphically.

The redshift evolution of the CDDF is usually parameterized by a power law $f(N_{\rm H\,I}, z) \propto (1+z)^\gamma$. However, observationally this γ appears to depend on $N_{\rm H\,I}$, implying that the shape of the CDDF evolves with time. The observational constraints on γ for $z \gtrsim 2$ in the Lyα forest regime ($N_{\rm H\,I} < 10^{17.2}$ cm^{-2}) are $\gamma \sim$ 2.0–3.0 from line-counting (Kim et al. 2002a) and measurements of the effective optical depth (Faucher-Giguère et al. 2008b; Dall'Aglio et al. 2008). The number densities of super-Lyman limit (10^{19} cm$^{-2} < N_{\rm H\,I} < 10^{20.3}$ cm^{-2}) and damped Lyα ($N_{\rm H\,I} > 10^{20.3}$ cm^{-2}) absorbers appear to evolve more slowly with $\gamma \sim 1.7$ (O'Meara et al. 2007; Worseck & Prochaska 2011) and ~ 1.27 (Rao et al. 2006), respectively. Rudie et al. (2013) found that their data were consistent with $\gamma = 2.5$ and 1.0 for $N_{\rm H\,I}$ below and above $\sim 10^{15}$ cm^{-2}, respectively.

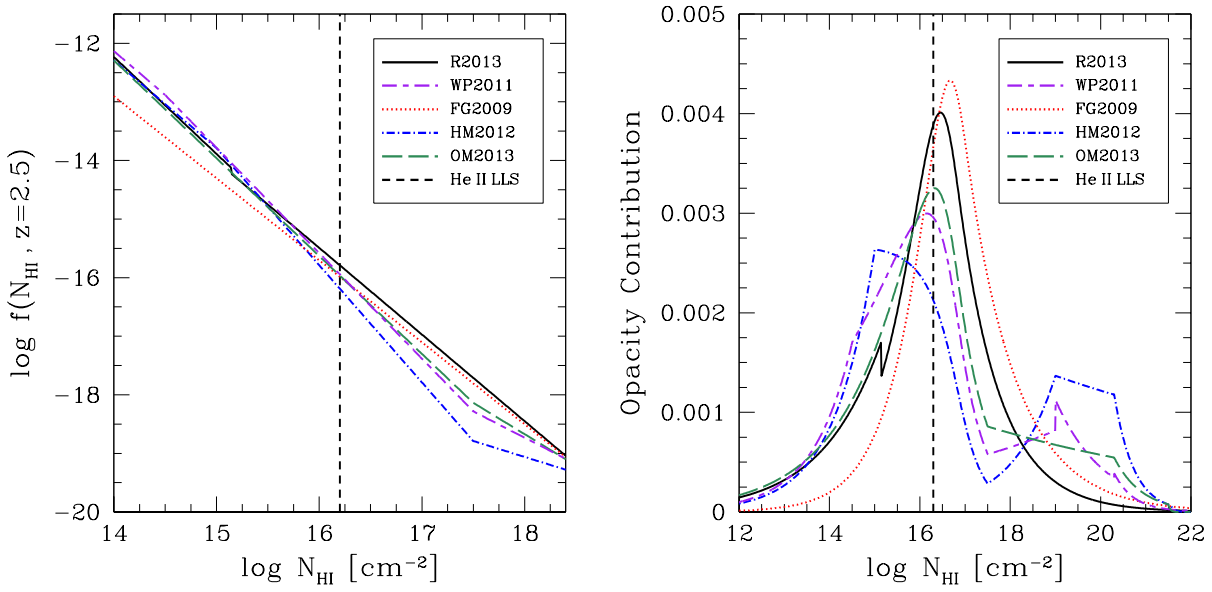

Figure 3. Left: Column density distribution functions $f(N_{\rm H\,I}, z = 2.5)$ considered in the text: Rudie et al. (2013) (solid black), Haardt & Madau (2012) (dot-dashed blue), Faucher-Giguère et al. (2009) (dotted red), O'Meara et al. (2013) (long-dashed green), Worseck & Prochaska (2011) (short-dashed-long-dashed purple), focusing on $N_{\rm H\,I}$ that correspond to the most important He II absorbers. The vertical dashed line shows the $N_{\rm H\,I}$ corresponding to a He II "LLS". Right: Relative contribution to the continuum opacity at $\nu_{\rm He\,II}$ per log($N_{\rm H\,I}$).

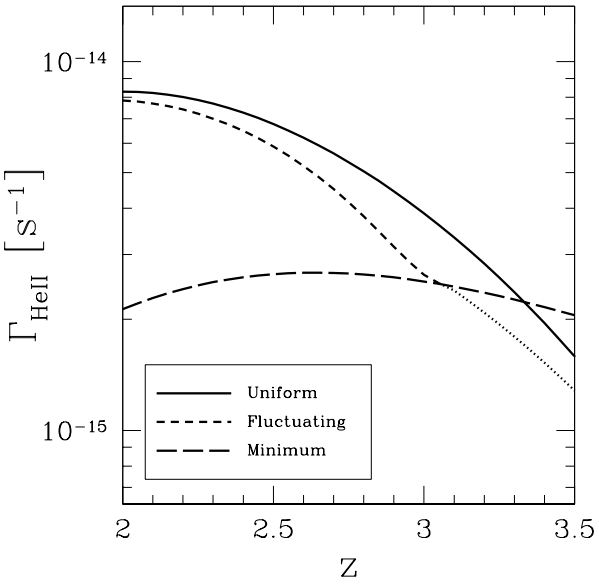

Figure 4. Uniform and fluctuating $\Gamma_{\rm He\,II}$ in the fiducial model (solid and dashed curves, respectively) and the "minimum" average ionization rate from isolated quasar profiles (long-dashed). The dotted curve represents the result of the fluctuating model calculation when it is inconsistent (i.e. below) the minimum background model from §2.4.

Worseck & Prochaska (2011) and Haardt & Madau (2012) compiled these observations (with the exception of Rudie et al. 2013) and constructed similar multi-step power law CDDFs. The primary difference between the two is the enhanced redshift evolution ($\gamma = 3.0$) of Lyα forest absorbers in the Haardt & Madau (2012) model compared to the Worseck & Prochaska (2011) model ($\gamma = 2.04$). Both models determine the redshift evolution of the CDDF by comparing to observations of the evolution of the H I Lyα effective optical depth, which is proportional to $(1+z)^{\gamma+1}$. However, Haardt & Madau (2012) calibrate to the measurements of Faucher-Giguère et al. (2008b), while Worseck & Prochaska (2011) chose the measurements of Dall'Aglio et al. (2008). It is unclear why such a difference exists in the effective optical depth evolution measured by these two groups, but it does not significantly affect our results.

In the following sections, we use the broken power-law CDDF from Rudie et al. (2013) as our fiducial model. Their model represents the first solid measurement of intermediate H I column density absorbers that are critical to the He II ionizing opacity, and is consistent with measurements of the H I Lyα effective optical depth (G. Rudie, priv. comm.). However, as the following sections will show, our choice of CDDF does not have significant implications for our final results, given the overall uncertainty in the amplitude of the ionizing background.

3 EVOLUTION OF THE IONIZING BACKGROUND

3.1 The Ionizing Background With Uniform Emissivity

The solid curve in Figure 4 shows how the He II ionization rate ($\Gamma_{\rm He\,II}$) evolves in our *uniform* fiducial model, ignoring fluctuations in the ionizing background. The uniform background model results in a steeply evolving ionizing background from $z \sim 3$–2, with an ionization rate that increases by a factor of ~ 2 over that range before flattening out substantially at later times. In the following sections, we discuss how variations in the input parameters affect this result.

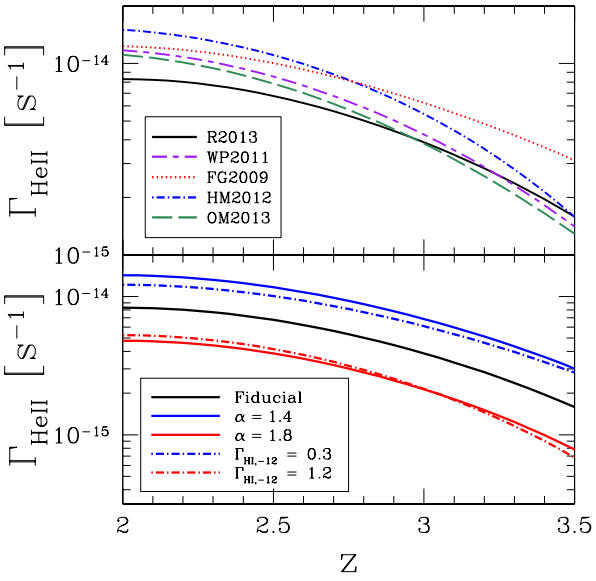

Figure 5. Top: $\Gamma_{\rm He\,II}$ in the uniform background model calculated for CDDFs from Figure 3. Bottom: Effect of assumed average quasar spectrum shortward of 912 Å, given by $F_\nu \propto \nu^{-\alpha}$ (solid curves), and assumed (constant) $\Gamma_{\rm H\,I}$ (dot-dashed curves).

3.1.1 *Column Density Distribution*

We considered a variety of CDDFs in our model. The top panel of Figure 5 shows the uniform ionizing background calculated with CDDFs used in earlier ionizing background calculations by Haardt & Madau (2012) and Faucher-Giguère et al. (2009), the direct measurement at $\langle z \rangle \sim 2.4$ by Rudie et al. (2013), and indirect extrapolation from higher redshift opacity measurements (Worseck & Prochaska 2011; O'Meara et al. 2013). In general, despite the significant differences between CDDFs apparent in the left panel of Figure 3, the evolution of the uniform background from $z = 3$–2 is fairly insensitive to the CDDF. The most significant differences are due to the different redshift evolution of the CDDFs, which is not very well constrained.

The right panel of Figure 3 shows the relative contribution to the ionizing continuum opacity at the He II edge as a function of $N_{\rm H\,I}$. Most of the opacity is due to He II "LLSs" with $N_{\rm He\,II} \sim \sigma_{\rm He\,II}^{-1}$, but the multi-step power law CDDFs have an increased contribution from relatively low $N_{\rm H\,I}$ ($\lesssim 10^{15}$ cm^{-2}) absorbers compared to the shallow power law Faucher-Giguère et al. (2009) CDDF. The H I column density corresponding to the peak He II opacity contribution varies from 10^{15} to $10^{16.7}$ cm^{-2} depending on the shape of the CDDF.

Figure 5 also shows that the normalization of $\Gamma_{\rm He\,II}$ depends sensitively on the total opacity calculated from the CDDF, which can vary significantly between models. If $\Gamma_{\rm He\,II}$ were accurately measured near $z \sim 2$, that measurement could in principle be used to help distinguish between models. However, measuring $\Gamma_{\rm He\,II}$ directly is extremely difficult, and as shown in the following sections, the other model parameters can be adjusted to produce similar differences in the normalization. For example, measurements of both the $\eta_{\rm thin}$ parameter and $\Gamma_{\rm H\,I}$ could potentially be used to constrain acceptable normalizations of $\Gamma_{\rm He\,II}$ (because the expected He II Lyα opacity in the IGM depends strongly on the value of the former parameter; see equation 6), but the current constraints on these parameters are too weak, and the degeneracies are too strong, to distinguish between the models presented in this and the following sections.

3.1.2 *Quasar Spectrum*

To assess the effect of choosing different average far-ultraviolet quasar spectral indices, we fix the H I Lyman limit emissivity given by equation 19 and scale to He II ionizing photons by $\epsilon_\nu \propto \nu^{-\alpha}$. The solid curves in the bottom panel of Figure 5 show how the range of observed values of the quasar spectral index α affects the He II ionization rate. A harder spectrum, which produces more ionizing photons at $\nu_{\rm He\,II}$, results in a higher ionization rate. Fixing the emissivity at $\nu_{\rm He\,II}$ and changing the spectral index has very little effect on the resulting $\Gamma_{\rm He\,II}$. In contrast, we find that $\Gamma_{\rm He\,II}$ changes more strongly than linearly with $\epsilon_{\rm He\,II}$; this is because the absorber structure changes with the ionizing background (and hence the emissivity). In general, as $\Gamma_{\rm He\,II}$ increases, the H I column density corresponding to a He II LLS increases. Since $N_{\rm H\,I} f(N_{\rm H\,I}, z)$ is a decreasing function of $N_{\rm H\,I}$, the number density of He II LLSs, and thus the overall opacity, decreases. This behaviour is similar to the emissivity-Γ feedback studied by McQuinn et al. (2011). The redshift evolution of the background is affected by α as well, but the effect is subtle.

3.1.3 *H I Ionization Rate*

The dot-dashed curves in the bottom panel of Figure 5 show how the He II ionization rate is affected by the assumed value of $\Gamma_{\rm H\,I}$. The effect is similar to changing the number of He II ionizing photons, because both parameters modulate the ratio of He II to H I in absorbers. While the decrease in He II opacity with an increasing number of He II ionizing photons is straightforward in principle, the relationship between $\Gamma_{\rm H\,I}$ and $\Gamma_{\rm He\,II}$ is more subtle. Consider an optically thin absorber: if $\Gamma_{\rm H\,I}$ decreases, the amount of H I in a fixed physical structure will increase while the amount of He II stays the same. This shift of the H I column density corresponding to a He II LLS causes $\Gamma_{\rm He\,II}$ to change with $\Gamma_{\rm H\,I}$: if $\Gamma_{\rm H\,I}$ is larger, the $N_{\rm H\,I}$ corresponding to a He II LLS will decrease, so He II LLSs will be more numerous and the overall He II opacity will increase. $\Gamma_{\rm H\,I}$ appears to affect the redshift evolution more strongly than α.

3.1.4 *Mean Free Path*

The solid curve in Figure 6 shows the evolution of $\bar{\lambda}_{\rm He\,II}$ in the uniform model. We also show how $\lambda_{\rm H\,I}$ increases with cosmic time (dotted curve); for ease of comparison we scale this curve to $\bar{\lambda}_{\rm He\,II}$ at $z = 2$. In contrast to the power-law evolution of $\lambda_{\rm H\,I}$ (described by equation 13), $\bar{\lambda}_{\rm He\,II}$ evolves much faster than a simple power law.

The evolution of the mean free path at the He II ionizing edge in our fiducial model is well-approximated by a power law with an index that itself evolves as a power law,

$$\lambda_{\rm He\,II} \sim 188 \text{ comoving Mpc } \times \left(\frac{1+z}{3}\right)^{\zeta(z)} \quad (21)$$

$$\zeta(z) = -2.41 \times \left(\frac{1+z}{3}\right)^{1.92}. \quad (22)$$

This fit differs by no more than $\sim 3\%$ from our full numerical calculations over the redshift range $z = 2$–3.8, but we caution

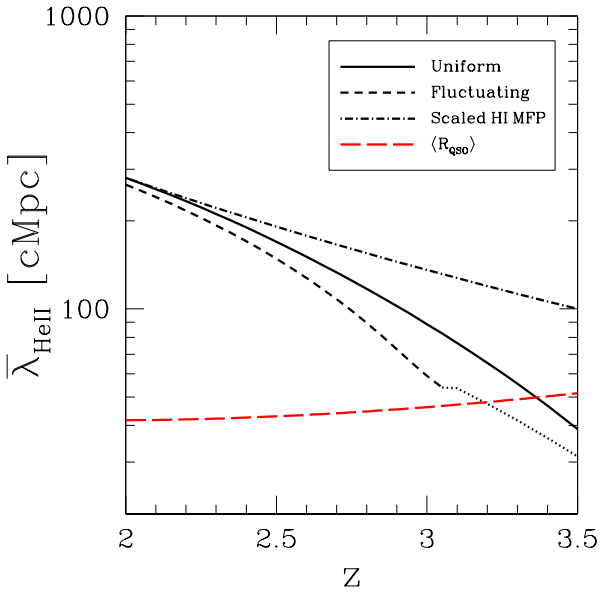

Figure 6. Evolution of the He II ionizing photon mean free path with redshift (black), evaluated at the average ionizing energy, for the uniform (solid) and fluctuating (dashed) models. The dotted curve represents the results of the fluctuating model when it is inconsistent with the minimum expected background from §2.4 as in Figure 4. The evolution of the hydrogen ionizing photon mean free path is shown as the dot-dashed curve, scaled to the He II mean free path at $z = 2$. The red long-dashed curve shows the average separation between luminous ($\nu_B L_B > 10^{11} L_\odot$) quasars given by the Hopkins et al. (2007) QLF.

the reader that the systematic uncertainties from our model input parameters are much, much larger than this. We also caution the reader against using this fit at $z \gtrsim 3.4$, where fluctuations in the ionizing background *must* be included (see below).

Because $\lambda_{\rm He\,II}$ is linked to $\Gamma_{\rm He\,II}$ through the absorber structure prescription, it evolves more quickly than $\lambda_{\rm H\,I}$. That is, increasing the mean free path increases the ionizing background, which will then increase the H I column density at which He II becomes optically thick, which in turn increases the mean free path, etc. This feedback effect is the fundamental source of the rapid evolution we see in $\Gamma_{\rm He\,II}$. (In fact, one could argue that it is strange that such rapid evolution does *not* occur in $\Gamma_{\rm H\,I}$; see McQuinn et al. 2011.)

The dependence of the mean free path on frequency is a function of the logarithmic slope of the CDDF, $\lambda_{\rm mfp} \propto \nu^{3(\beta-1)}$ (equation 13). The He II CDDF is not precisely defined in our model, but a mapping of our fiducial H I CDDF through our absorber prescription results in $\beta_{\rm He\,II} \sim 1.43$ for the absorbers that contribute the bulk of the opacity near the He II ionizing edge ($10^{14.5} \lesssim N_{\rm H\,I} \lesssim 10^{17.0}$ cm^{-2} as in Figure 3), and consequently $\lambda_{\rm He\,II} \propto \nu^{1.3}$ for $1 \leq \nu/\nu_{\rm He\,II} \lesssim 2.5$. $\bar{\nu}/\nu_{\rm He\,II} \sim 1.37$ is typical for our fiducial model, so $\bar{\lambda}_{\rm He\,II}/\lambda_{\rm He\,II} \sim 1.51$.

3.1.5 Recombination Photons

The fractional contribution of recombination emission to $\Gamma_{\rm He\,II}$ is fairly minor. In the absence of quasars, but with the opacity as a function of redshift fixed to the uniform model, recombination photons alone produce an ionization rate about $\sim$ 7–15% of the fiducial value. However, because the absorber population is sensitive to the emissivity (as in § 3.1.2), the relative difference between $\Gamma_{\rm He\,II}$ calculated with recombination emission and $\Gamma_{\rm He\,II}$ calculated without recombination emission is larger ($\sim$ 20–40%). While Faucher-Giguère et al. (2009) found that including recombination emission increased $\Gamma_{\rm He\,II}$ by only $\sim 10\%$, Figure 3 shows that their CDDF has a significant deficit of the optically thin ($N_{\rm H\,I} \lesssim 10^{16}$ cm^{-2}) systems that contribute most of the recombination emissivity.

In simple models of the reionization process, it is conventional to describe the enhanced recombination rate of ionized species n_i due to an inhomogeneous IGM through the so-called clumping factor, $C = \langle n_i n_e \rangle / (\langle n_i \rangle \langle n_e \rangle)$. Usually, this is estimated from simple phenomenological arguments or from the density structure in numerical simulations. However, these approaches are not entirely satisfactory, as the clumping factor should incorporate information that depends on the distribution of ionized and neutral patches. For example, recombinations that occur inside of dense, self-shielded systems do not produce photons that can ionize the IGM, as the resulting photons are trapped within the systems.

With our detailed model, we can estimate this factor for He III self-consistently (given a model for the emitting and absorbing populations) by explicitly following the fraction of recombinations that occur inside of self-shielded systems. In particular, we have

$$C_{\rm eff} = \frac{\int_{\nu_{\rm He\,II}}^{\infty} \epsilon_{\nu,{\rm rec}}/(h\nu) d\nu}{(\alpha^A_{\rm He\,II} - \alpha^B_{\rm He\,II}) \langle n_{\rm He\,III} \rangle \langle n_e \rangle}, \quad (23)$$

which describes the effective recombination rate after correcting for self-absorption of ionizing recombination photons within the emitting clouds relative to a uniform IGM. In our fiducial uniform model, $C_{\rm eff}$ increases from $C_{\rm eff} \sim 1$ at $z = 3.5$ to $C_{\rm eff} \sim 4$ at $z = 2$.

3.2 The Ionizing Background Including Fluctuations

It is instructive to compare the mean free path from the preceding section to the average separation between the primary sources of ionizing photons, bright quasars with $\nu_B L_B > 10^{11} L_\odot$. We calculate the number density of the bright quasars by integrating the Hopkins et al. (2007) luminosity function over this luminosity range and estimating their average separation by $\langle R \rangle \sim n^{-1/3}$. The long-dashed red curve in Figure 6 shows this separation; $\langle R \rangle \sim 45$ Mpc is a good approximation for the entire redshift interval from $z \sim$ 2–3.

When the mean free path is similar to the average source separation, fluctuations in the background contribute a substantial opacity excess. The dashed curve in Figure 4 shows the effect of these fluctuations on the ionizing background. Figure 7 shows that, compared to the uniform model, the fluctuating background model exhibits a $\sim$ 20–40% dip at $z \sim$ 3–3.2 for our fiducial input parameters and various CDDFs from § 3.1.1. The evolution of all the CDDF models, with the exception of the shallow slope model from Faucher-Giguère et al. (2009), is very similar. The "feedback" effect between the opacity and the ionizing background is weaker for shallower CDDF slopes (e.g. McQuinn et al. 2011), so the net effect of fluctuations is smaller in the Faucher-Giguère et al. (2009) model. The "recovery" of the fluctuating model at higher redshift relative to the uniform model is due to our minimum ionization rate approximation from Section 2.4 which limits the effective opacity to ionizing photons.

We note that there are two related sources for the differences between the curves in Figure 7: the shape of the column density dis-

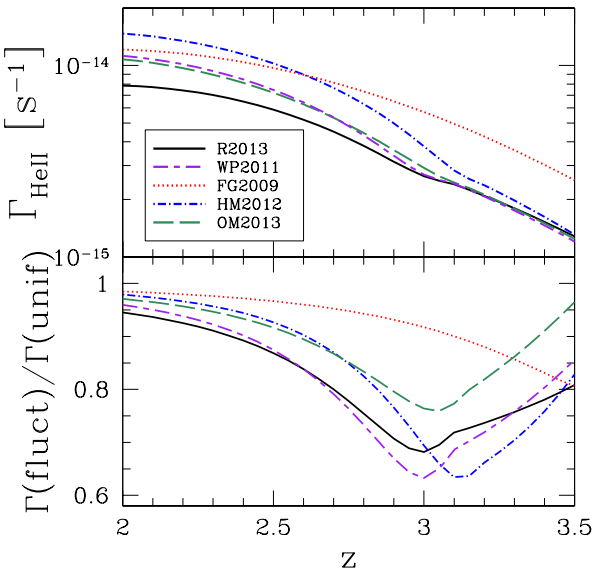

Figure 7. Top: Fluctuating model ionization rate for the same CDDFs as Figure 3. Bottom: Ratio of the fluctuating and uniform model ionization rates.

tributions and the normalization of the ionizing background. Leaving the CDDF shape fixed, different choices for the ionizing emissivity result in very similar shapes to those in Figure 7, though the redshift above which the minimum background is larger than the fluctuating background will shift depending on the relative normalization of the two models. The more subtle differences in the shapes of the curves are due to variations in the shape of the CDDF; this is most dramatically seen by the dotted curve (which is only below the minimum background model at $z \gtrsim 3.8$).

The most important effect of including fluctuations is to induce a more rapid increase in $\Gamma_{\rm He\,II}$ with cosmic time. Consider a region with a smaller than average emissivity. In that region, the ionizing background will also be smaller, so each absorber will be more optically thick and the mean free path will be smaller. This will further decrease the ionizing background, etc. In a realistic model of the distribution of $\Gamma_{\rm He\,II}$ in the presence of quasars, most of the volume of the universe has an ionizing background a few times *below* the universal average (to compensate for the very brightly illuminated, but small, regions around quasars; see Figure 1). Thus, the average opacity through the universe is higher, decreasing the resulting mean ionizing background.

The turndown from the uniform model is thus a straightforward and robust prediction of our fluctuating background model, though its magnitude depends on the CDDF. At higher redshift ($z \gtrsim 3$), it is clear that the He II ionizing background evolution should no longer be described by a cosmological radiative transfer model without properly taking into account the effect of localized transparent regions around sources. Our simple analytic model for the minimum ionization rate from isolated quasars, the minimum background model, should represent a fairly strict lower limit to the ionizing background in the post-reionization (i.e. ionization equilibrium) limit. If this is indeed the case, one might expect the volume-averaged ionization rate to evolve *more slowly* at higher redshift ($z \gtrsim 3.1$) than predicted by standard cosmological radiative transfer. While our minimum model neglects a diffuse partially-neutral component to the IGM that should exist prior to the completion of He II reionization, this slower evolution is consistent with the He II reionization simulations of McQuinn et al. (2009) and with expectations from hydrogen reionization (Furlanetto & Mesinger 2009). In both cases, the ionizing background is reduced to a set of independent "proximity zones" (though for different reasons), with the mean background depending principally on the filling factor of these regions.

These calculations show that the ionizing background can evolve very rapidly at $z \lesssim 3$, *even without any assumptions about an evolving He II fraction*. The precise degree of evolution is uncertain, but it is at least a factor of a few–even in the standard uniform emissivity model–and likely nearly a factor of five when fluctuations are included. In other words, even without late He II reionization, we should see a rapid increase in the intensity of the metagalactic radiation field. This evolution is in stark contrast to observations of the H I ionization rate, which appears to be roughly constant from $z \sim 2$–4; this difference is most likely due to the increasing influence (towards higher redshift) of star-forming galaxies (as opposed to quasars) to the H I ionizing emissivity. We will consider the observable implications of this conclusion in the following section.

For $z \lesssim 3$, the mean free path at the He II ionizing edge in the fluctuating background model is well-characterized by a similar power law within a power law as the uniform model (equation 21),

$$\lambda_{\rm He\,II} \sim 178 \text{ comoving Mpc } \times \left(\frac{1+z}{3}\right)^{\zeta(z)} \quad (24)$$

$$\zeta(z) = -2.64 \times \left(\frac{1+z}{3}\right)^{2.61}. \quad (25)$$

The primary difference between the uniform and fluctuating background fits is the larger power law index of $\zeta(z)$, a consequence of faster ionizing background evolution. As discussed previously, the mean free path of average energy ionizing photons that we use in the fluctuating background calculation is somewhat larger:

$$\bar{\lambda}_{\rm He\,II} \sim 266 \text{ comoving Mpc } \times \left(\frac{1+z}{3}\right)^{\zeta(z)} \quad (26)$$

$$\zeta(z) = -2.62 \times \left(\frac{1+z}{3}\right)^{2.38}. \quad (27)$$

4 EFFECTIVE OPTICAL DEPTH

To gauge the observable import of our results, we will briefly consider how they manifest in the evolution of the IGM opacity to far-ultraviolet photons. He II Lyα absorption has been measured in far-ultraviolet spectra from $z \sim 2$–4 (Dixon & Furlanetto 2009 and references therein; Worseck et al. 2011; Syphers et al. 2011, 2012; Syphers & Shull 2013). We will compare to the most basic observable from the resulting forest of observed absorption features, the average optical depth $\tau_{\rm eff}$ for the He II Lyα transition. We use two different methods to predict $\tau_{\rm eff}$: a semi-analytic model using a gas density probability distribution $P(\Delta)$ as in Dixon & Furlanetto (2009), and a direct integration of the He II Lyα opacity from the H I CDDF and our absorber structure prescription.

Under the assumptions of a highly-ionized universe in ionization equilibrium, line opacity dominated by zero-width optically thin absorbers, and a power-law temperature-density relation $T = T_0 \Delta^{1-\gamma_d}$, the He II Gunn-Peterson optical depth can be expressed as (Dixon & Furlanetto 2009)

$$\tau_{\rm GP} \simeq 13.6\kappa \left(\frac{\Gamma_{\rm He\,II}}{10^{-14}\,{\rm s}^{-1}}\right)^{-1} \left(\frac{T_0}{10^4\,{\rm K}}\right)^{-0.7} \left(\frac{\Omega_b h^2}{0.0241}\right)^2$$

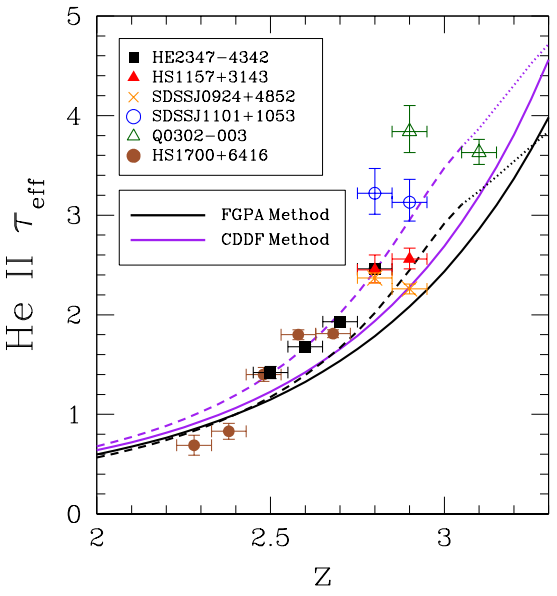

Figure 8. Effective optical depth for the uniform (solid), fluctuating (dashed), "plateau" (dotted), and "minimum" (dash-dotted) models, using the FGPA (black) and CDDF (purple) methods. The points are $\Delta z = 0.1$-binned effective optical depth data for various quasar sightlines from Syphers & Shull (2013) ((HS1700+6416, filled brown circles; excluding metal absorption) and Worseck et al. (2011) (G. Worseck, priv. comm.; HE2347-4342, black squares; HS1157+3143, filled red triangles; SDSSJ0924+4852, orange crosses; SDSSJ1101+1053, open blue circles; Q0302-003, open green triangles).

$$\times \left(\frac{\Omega_m h^2}{0.142}\right)^{-1/2} \left(\frac{1+z}{4}\right)^{9/2} \Delta^{2-0.7(\gamma_d-1)}. \quad (28)$$

This "fluctuating Gunn-Peterson approximation" (FGPA; Weinberg et al. 1997) relates the continuum optical depth to the local overdensity Δ and ionization rate $\Gamma_{\rm He\,II}$. The systematic uncertainty in $\tau_{\rm GP}$ due to the above simplifications is collapsed into a normalization constant κ, which we calibrate to (one of) the observations. We assume an isothermal temperature-density relation ($\gamma_d = 1$) for simplicity, but this does not affect our results significantly. Assuming the gas density probability distribution given by Miralda-Escudé et al. (2000), we then calculate $\tau_{\rm eff}$ by integrating over the density and ionization rate distributions:

$$e^{-\tau_{\rm eff}} = \int_0^\infty d\Gamma f(\Gamma) \int_0^\infty d\Delta e^{-\tau_{\rm GP}(\Gamma,\Delta)} P(\Delta). \quad (29)$$

We normalized the FGPA results for the uniform and fluctuating models to produce an optical depth of $\tau = 1.0$ at $z = 2.4$ to roughly match observations (Worseck et al. 2011; Syphers & Shull 2013) when the expected variation between sightlines is small. These normalizations require $\kappa = 1.56$ and $\kappa = 1.28$ (equation 28) for the uniform and fluctuating models, respectively.

An alternative method to calculate $\tau_{\rm eff}$ is to directly integrate the He II Lyα opacity from the CDDF. The only additional information needed is the distribution of line widths, provided by the Doppler parameter b. In this method, $\tau_{\rm eff}$ is given by (Zuo 1993)

$$\tau_{\rm eff} = \frac{1+z}{\lambda_{\rm He\,II,Ly\alpha}} \times \int_{N_{\rm H\,I,min}}^{N_{\rm H\,I,max}} dN_{\rm H\,I} \int_0^\infty db f(N_{\rm H\,I}, b) W(N_{\rm H\,I}, b), \quad (30)$$

where $W(N_{\rm H\,I}, b)$ is the He II Lyα equivalent width of an absorber with Doppler parameter b and $f(N_{\rm H\,I}, b)$ is the joint distribution of $N_{\rm H\,I}$ and b. We assume that $N_{\rm H\,I}$ and b are uncorrelated and that the distribution of b is a Dirac-delta function at $b = 30$ km s^{-1}, a representative approximation for H I Lyα forest systems (Kim et al. 2001). In this method we do not subject the resulting optical depth to any extra normalization.

The results of the FGPA and CDDF methods are shown in Figure 8. Both methods demonstrate that steep evolution of $\Gamma_{\rm He\,II}$ naturally leads to steep evolution in the observed $\tau_{\rm eff}$. The addition of fluctuations further accelerates the evolution. The results for different input parameters (α, $\Gamma_{\rm H\,I}$, CDDF) are largely the same in the FGPA method when normalized at $z = 2.4$. In contrast, the CDDF method depends sensitively on $\eta_{\rm thin} \propto \Gamma_{\rm H\,I}/\Gamma_{\rm He\,II}$ (equation 6), which can differ by a factor of a few between models. Thus, for a given CDDF, the He II optical depth places a joint constraint on $\Gamma_{\rm H\,I}$ and α, subject to the uncertainties inherent in our cosmological radiative transfer model.

For context, we also show measured $\tau_{\rm eff}$ points in Figure 8 from Syphers & Shull (2013) and Worseck et al. (2011). These two works determine the effective optical depth by measuring the transmission uniformly across the redshift interval ($\tau_{\rm eff} = -\ln\langle F\rangle$) instead of averaging transmission from sparse redshift coverage provided by past works (Dixon & Furlanetto 2009) or averaging pixel optical depths (Shull et al. 2010). It is interesting that our models – which explicitly ignore He II reionization – match the evolution in the observed optical depth rather well. Additionally, the fluctuating background models appear to match the observations more closely than the uniform models, especially at $z \gtrsim 2.7$ where the observed optical depth evolution is very steep. Our result demonstrates that the observed trend in and of itself does not *require* the He II fraction to evolve, although it also does not rule out such evolution.

Unfortunately, our models do not explicitly describe how the integrated $\tau_{\rm eff}$ should vary at the same redshift along different lines of sight, even when averaged over large path lengths. This is because our model assumes that the high and low Γ regions are distributed perfectly randomly, without the spatial correlations between them that are essential to understanding the observed averages (Furlanetto & Dixon 2010). Hydrodynamic simulations by McQuinn et al. (2009) and semi-analytic models by Furlanetto & Dixon (2010) have described spatial variations in $\tau_{\rm eff}$. Interestingly, the well-studied spectrum of HE 2347–4342 (Reimers et al. 1997; Kriss et al. 2001; Zheng et al. 2004; Shull et al. 2004, 2010) shows regions of high optical depth that appear to require large swathes of He II at $2.7 \lesssim z \lesssim 2.9$. We therefore emphasize that our models do not demand that He II reionization be over by $z \sim 3$; they instead demonstrate that, with respect to the evolution of the mean opacity, it is not required.

5 DISCUSSION

Our model for background fluctuations increases the average opacity of the IGM when the mean free path is comparable to the separation between bright sources. This effect is primarily due to the skewness of $f(\Gamma)$ towards lower Γ as the mean free path decreases (as in Figure 1). While the effect of our fluctuations prescription on the ionizing background is relatively small, it predicts a steep increase in the ionizing background when the background transitions

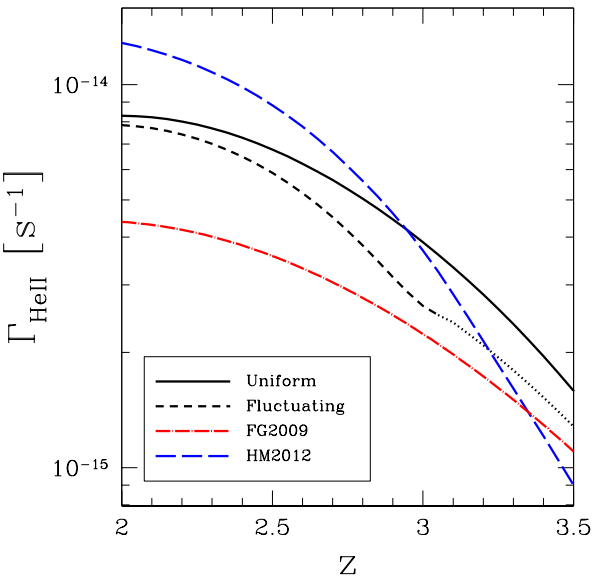

Figure 9. Uniform (solid black) and fluctuating (dashed black) He II ionization rate from this work compared to the models from Haardt & Madau (2012) (long-dashed blue) and Faucher-Giguère et al. (2009) (long-dash-dotted red).

from being dominated by local sources to a smoother background with contributions from distant sources.

5.1 Comparison to past theoretical work

Figure 9 shows how our model compares to a pair of recent ionizing background calculations by Haardt & Madau (2012) and Faucher-Giguère et al. (2009).

Faucher-Giguère et al. (2009) used a single power-law CDDF with $\beta = 1.4$ and $\gamma = 1.5$ that severely underestimates the number of low-density Lyα forest absorbers compared to recent observations (see the left panel of Figure 3) and evolves more slowly than implied by Lyα forest measurements (Kim et al. 2002a). Because their CDDF severely underestimates the H I opacity of the IGM from sub-LLS absorbers, they were forced to renormalize the quasar emissivity of ionizing photons at the hydrogen ionizing edge by a factor of 0.36 to match their measured $\Gamma_{\rm H\,I} \sim 0.5 \times 10^{-12}$ s^{-1} (Faucher-Giguère et al. 2008a), and thus their $\Gamma_{\rm He\,II}$ is normalized somewhat lower as well. Their $\Gamma_{\rm He\,II}$ evolves at a similar rate to our fiducial uniform background model.

Haardt & Madau (2012) used a CDDF that evolves more rapidly with redshift than our fiducial model and calculated a $\Gamma_{\rm H\,I}$ that peaks at $z \sim 2$ and declines slowly towards higher redshift. They also used a different fitting form for the structure of IGM absorbers. In their fit they more accurately approximated the average ionization rate within absorbers, which resulted in a more accurate fit to η at large H I column densities. However, as mentioned previously in § 2.1.1, those high $N_{\rm H\,I}$ systems do not contribute a substantial fraction of the opacity near the He II edge, and thus our approximation should not significantly affect our results.

5.2 Fluctuating Model Caveats

Other than the general simplifications necessary to invoke the cosmological radiative transfer model, our parameterization of the fluctuations in the background is an ad hoc addition to a model designed for a medium with a uniform emissivity. In this section, we describe the primary uncertainties with such an approach.

First of all, we may not have accurately captured the extent and character of the fluctuations. Spatial correlations in the ionizing background exist due to the large proximity regions of the primary sources (as seen in the minimum model of § 2.4). It is possible that a full characterization of the ionizing background fluctuations including proximity effects would negate the need to separately consider the minimum background due to isolated sources, though obviously such an effort is different. Additionally, the massive hosts of these luminous quasars are clustered, which will increase the amplitude of the fluctuations. However, the proximity zones of the quasars are so large, and the quasars so rare, that stochastic variations dominate over large-scale clustering in all reasonable scenarios anyway (Dixon et al. 2013). The absorbers also show some clustering (Rudie et al. 2012, 2013) which will modulate the metagalactic radiation field (although likely only modestly).

Other obvious sources of additional fluctuations in the ionizing background – over and above those from the discrete sources – include radiative transfer effects (e.g. "shadows" behind optically thick regions as in Tittley & Meiksin 2007) and collisional ionization in superheated shocks (Muzahid et al. 2011). Of course, incomplete He II reionization may leave opaque patches of He II that would introduce severe fluctuations (McQuinn et al. 2009; Furlanetto & Dixon 2010) which have possibly been observed recently (Zheng et al. 2004; Shull et al. 2010; Worseck et al. 2011). We have explicitly ignored this possibility here so as to consider the evolution of the ionizing background in the absence of such effects.

We also treat recombinations only approximately. We include recombination emission in our fluctuating model calculation in the same way as in the uniform model, by simply adding to the pre-existing quasars' emissivity. It therefore implicitly has the same source distribution, while in fact it will be more uniform than the point-like quasars because it is distributed throughout the IGM. On the other hand, recombination emission in low $\Gamma_{\rm He\,II}$ regions will be weaker, and much of the emission from high $\Gamma_{\rm He\,II}$ regions (i.e. near bright quasars) will not travel much beyond those quasar proximity regions before redshifting below $\nu_{\rm He\,II}$ ($\lesssim$30 Mpc; § 2.1.2), so its effect on $f(\Gamma)$ should be fairly minor.

6 CONCLUSION

We have calculated the He II ionizing background using a cosmological radiative transfer model that takes into account the latest constraints on quasar and IGM source properties. In our uniform background model, which closely mimics previous work (Fardal et al. 1998; Faucher-Giguère et al. 2009; Haardt & Madau 2012), we found that the He II ionization rate, $\Gamma_{\rm He\,II}$, and the mean free path of He II ionizing photons should both evolve significantly during the time after He II reionization ($z \sim 2-3$). However, at $z \sim 3$, the mean free path of He II ionizing photons is comparable to the average distance between the bright quasars that contribute most of the ionizing emissivity. While previous work investigated how this effect introduces fluctuations in the ionizing background (Fardal et al. 1998; Meiksin & White 2003; Furlanetto 2009), its

implications for the *mean* ionizing background itself have not been studied in detail until now.

We investigated for the first time how these fluctuations can affect the evolution of the mean background. We incorporated the distribution $f(\Gamma)$ into our cosmological radiative transfer model by averaging the opacity to He II ionizing photons over it. However, that procedure still models the emission as diffuse sources rather than point-like quasars, so we supplemented it with a physical model that accounts for the decreased average opacity at high redshift by considering *isolated* transparent zones around individual quasars. Including that model, our results showed that the fluctuating background introduces another source of opacity which causes the ionization rate to decrease by a factor of $\sim 30\%$ at $z \sim 3.1$ relative to the uniform background calculation. For $z \gtrsim 3.1$, the cosmological radiative transfer model predicts a mean background below the minimum model, suggesting that it is no longer adequate to properly model the evolution of the He II ionizing background at those redshifts.

As an example of the utility of our ionizing background model, we used the resulting ionization rate to estimate the evolution of the He II Lyα effective optical depth, $\tau_{\rm eff}$. Rapid evolution at $z \gtrsim 2.5$, similar to that seen in observations, appears to be a natural consequence of a steeply evolving ionization rate. The addition of fluctuations improves our model's resemblance to the observed $\tau_{\rm eff}$ evolution somewhat, though systematic uncertainties in the data analysis make a detailed comparison difficult.

We note that our model does not incorporate He II reionization: that is, we assume that the He II fraction is very small throughout the IGM. We have therefore shown that reionization is not the *only* possible cause of a rapidly evolving ionizing background. Instead, the interaction between the (slowly) increasing emissivity and the (slowly) evolving IGM clumpiness can feed back on each other, strongly amplifying the evolution of the ionizing background. Such evolution is naively predicted by simple models (McQuinn et al. 2011) but is not observed in the hydrogen-ionizing background at these redshifts.

Our result emphasizes the importance of understanding the IGM for interpreting measurements of the ionizing background and of reionization, including that of both He II and H I . In the context of He II reionization, Dixon & Furlanetto (2009) argued that the rapidly increasing mean optical depth in the He II Lyα line is consistent with ongoing He II reionization at $z \gtrsim 2.7$. However, they prescribed a relatively slow evolution in the mean free path of ionizing photons. On the other hand, a number of observations show substantial fluctuations in the mean optical depth, even when averaged over large scales (Reimers et al. 1997; Zheng et al. 2004; Shull et al. 2004, 2010). Our model does not address such large-scale fluctuations, because we have not incorporated any spatial information into the calculation.

This calculation may also have important implications for H I reionization, where an apparent rapid increase in the H I Lyα optical depth has long been attributed to the tail end of reionization (Fan et al. 2002, 2006). Furlanetto & Mesinger (2009) previously showed that the overlap process of reionization (when ionized bubbles overlap to fill space) does not by itself cause a rapid increase in the ionizing background. We have shown that such an increase can be caused by "normal" post-reionization processes, through the interaction of a slowly increasing emissivity and slowly decreasing IGM clumping. Whether this occurs during H I reionization cannot be said, because it depends sensitively on the evolution of that clumping (which is largely hidden due to the high opacity of the Lyα forest beyond $z \sim 6$). However, this He II analog indicates that a proper interpretation of data regarding H I reionization requires careful modelling (and ideally observations) of the IGM and not simply an understanding of the emitting sources.

We thank K. Dixon, G. Rudie, C. Steidel, D. Syphers, and G. Worseck for helpful conversations, and the anonymous referee for many helpful comments. We also thank G. Worseck for providing $\Delta z = 0.1$ effective optical depth data. This research was partially supported by the David and Lucile Packard Foundation and the Alfred P. Sloan Foundation.

REFERENCES

Aguirre A., Schaye J., Kim T.-S., Theuns T., Rauch M., Sargent W. L. W., 2004, ApJ, 602, 38
Bolton J. S., Haehnelt M. G., 2007, MNRAS, 382, 325
Bolton J. S., Haehnelt M. G., Viel M., Carswell R. F., 2006, MNRAS, 366, 1378
Bolton J. S., Haehnelt M. G., Viel M., Springel V., 2005, MNRAS, 357, 1178
Bolton J. S., Viel M., 2011, MNRAS, 414, 241
Dall'Aglio A., Wisotzki L., Worseck G., 2008, A&A, 491, 465
Davé R., Hernquist L., Katz N., Weinberg D. H., 1999, ApJ, 511, 521
Dixon K. L., Furlanetto S. R., Mesinger A., 2013, ArXiv e-prints
Dixon K. L., Furlanetto S. R., 2009, ApJ, 706, 970
Dunkley J. et al., 2009, ApJS, 180, 306
Fan X., Narayanan V. K., Strauss M. A., White R. L., Becker R. H., Pentericci L., Rix H.-W., 2002, AJ, 123, 1247
Fan X. et al., 2006, AJ, 132, 117
Fardal M. A., Giroux M. L., Shull J. M., 1998, AJ, 115, 2206
Faucher-Giguère C.-A., Lidz A., Hernquist L., Zaldarriaga M., 2008a, ApJ, 682, L9
Faucher-Giguère C.-A., Lidz A., Zaldarriaga M., Hernquist L., 2009, ApJ, 703, 1416
Faucher-Giguère C.-A., Prochaska J. X., Lidz A., Hernquist L., Zaldarriaga M., 2008b, ApJ, 681, 831
Furlanetto S. R., 2009, ApJ, 703, 702
Furlanetto S. R., Dixon K. L., 2010, ApJ, 714, 355
Furlanetto S. R., Mesinger A., 2009, MNRAS, 394, 1667
Furlanetto S. R., Oh S. P., 2008, ApJ, 681, 1
Haardt F., Madau P., 1996, ApJ, 461, 20
Haardt F., Madau P., 2012, ApJ, 746, 125
Hopkins P. F., Richards G. T., Hernquist L., 2007, ApJ, 654, 731
Kim T.-S., Carswell R. F., Cristiani S., D'Odorico S., Giallongo E., 2002a, MNRAS, 335, 555
Kim T.-S., Cristiani S., D'Odorico S., 2001, A&A, 373, 757
Kim T.-S., Cristiani S., D'Odorico S., 2002b, A&A, 383, 747
Kriss G. A. et al., 2001, Science, 293, 1112
Madau P., Haardt F., Rees M. J., 1999, ApJ, 514, 648
McDonald P., Miralda-Escudé J., 2001, ApJ, 549, L11
McQuinn M., Lidz A., Zaldarriaga M., Hernquist L., Hopkins P. F., Dutta S., Faucher-Giguère C.-A., 2009, ApJ, 694, 842
McQuinn M., Oh S. P., Faucher-Giguère C.-A., 2011, ApJ, 743, 82
Meiksin A., 2009, Rev. Mod. Phys., 81, 1405
Meiksin A., White M., 2003, MNRAS, 342, 1205
Meiksin A., White M., 2004, MNRAS, 350, 1107
Miralda-Escude J., 1993, MNRAS, 262, 273
Miralda-Escudé J., Haehnelt M., Rees M. J., 2000, ApJ, 530, 1
Muzahid S., Srianand R., Petitjean P., 2011, MNRAS, 410, 2193
O'Meara J. M., Prochaska J. X., Burles S., Prochter G., Bernstein R. A., Burgess K. M., 2007, ApJ, 656, 666
O'Meara J. M., Prochaska J. X., Worseck G., Chen H.-W., Madau P., 2013, ApJ, 765, 137
Paresce F., McKee C. F., Bowyer S., 1980, ApJ, 240, 387
Paschos P., Norman M. L., Bordner J. O., Harkness R., 2007, ArXiv e-prints

Prochaska J. X., O'meara J. M., Worseck G., 2010, ApJ, 718, 392
Prochaska J. X., Worseck G., O'meara J. M., 2009, ApJL, 705, L113
Rao S. M., Turnshek D. A., Nestor D. B., 2006, ApJ, 636, 610
Rauch M., 1998, ARAA, 36, 267
Rauch M. et al., 1997, ApJ, 489, 7
Reimers D., Kohler S., Wisotzki L., Groote D., Rodriguez-Pascual P., Wamsteker W., 1997, A&A, 327, 890
Rudie G. C., Steidel C. C., Shapley A. E., Pettini M., 2013, ApJ, 769, 146
Rudie G. C. et al., 2012, ApJ, 750, 67
Schaye J., 2001, ApJ, 559, 507
Scott J., Bechtold J., Dobrzycki A., Kulkarni V. P., 2000, ApJS, 130, 67
Scott J. E., Kriss G. A., Brotherton M., Green R. F., Hutchings J., Shull J. M., Zheng W., 2004, ApJ, 615, 135
Shull J. M., France K., Danforth C. W., Smith B., Tumlinson J., 2010, ApJ, 722, 1312
Shull J. M., Stevans M., Danforth C. W., 2012, ApJ, 752, 162
Shull J. M., Tumlinson J., Giroux M. L., Kriss G. A., Reimers D., 2004, ApJ, 600, 570
Sokasian A., Abel T., Hernquist L., 2003, MNRAS, 340, 473
Songaila A., 1998, AJ, 115, 2184
Songaila A., 2005, AJ, 130, 1996
Springel V., Hernquist L., 2003, MNRAS, 339, 312
Syphers D., Anderson S. F., Zheng W., Meiksin A., Haggard D., Schneider D. P., York D. G., 2011, ApJ, 726, 111
Syphers D., Anderson S. F., Zheng W., Meiksin A., Schneider D. P., York D. G., 2012, AJ, 143, 100
Syphers D., Shull J. M., 2013, ApJ, 765, 119
Telfer R. C., Zheng W., Kriss G. A., Davidsen A. F., 2002, ApJ, 565, 773
Tittley E. R., Meiksin A., 2007, MNRAS, 380, 1369
Tytler D., 1987, ApJ, 321, 49
Weinberg D. H., Hernsquit L., Katz N., Croft R., Miralda-Escudé J., 1997, in Structure and Evolution of the Intergalactic Medium from QSO Absorption Line System, Petitjean P., Charlot S., eds., p. 133
Worseck G., Prochaska J. X., 2011, ApJ, 728, 23
Worseck G. et al., 2011, ApJL, 733, L24
Zheng W. et al., 2004, ApJ, 605, 631
Zuo L., 1992, MNRAS, 258, 36
Zuo L., 1993, A&A, 278, 343